

Fuzzy Gain–Enhanced Shunt Active Power Filter for Harmonic Suppression in A 33-kV Nigerian Distribution Feeder: Afaha-Ube–Manta 1 Case Study

Patience J. Sunday^{1*}, Nseobong I. Okpura², Unwana I. Ibang³

^{1,2,3}Department of Electrical/Electronics Engineering, University of Uyo, Uyo, Nigeria

*Corresponding Author

Date of Submission: 27-03-2026

Date of Acceptance: 06-04-2026

ABSTRACT: This paper presents a harmonic-mitigation study for a 33-kV medium-voltage distribution feeder (Afaha-Ube substation to Manta 1, 32 km) using a shunt active power filter (SAPF) strengthened with a fuzzy gain-enhancement layer. The feeder and nonlinear load were modelled in MATLAB/Simulink, and harmonic performance was evaluated at the sending and receiving buses using IHD and THD indices. In the uncompensated condition, the network exhibited double-digit current distortion and elevated voltage distortion (Bus 1: THD_I = 12.31%, THD_V = 9.41%; Bus 2: THD_I = 12.87%, THD_V = 8.99%). Introducing a standalone SAPF reduced distortion to low-single-digit levels (Bus 1: 4.19% / 3.65%; Bus 2: 4.23% / 3.01% for current/voltage THD), while the proposed SAPF–fuzzy scheme achieved sub-1% current THD with approximately 1% voltage THD (Bus 1: 0.48% / 1.11%; Bus 2: 0.67% / 0.97%), demonstrating a clear incremental benefit of fuzzy gain adaptation over fixed-parameter active filtering for MV feeder power-quality improvement.

KEYWORDS: Shunt active power filter; fuzzy logic control; harmonic mitigation; total harmonic distortion; 33-kV distribution feeder

I. INTRODUCTION

Harmonic mitigation in practice spans passive and active solutions. Passive filters remain attractive for their simplicity and reactive-power support, yet their performance can be sensitive to network impedance variations, detuning, and resonance risks under changing operating conditions. Contemporary distribution-focused reviews emphasize that active compensation technologies (including shunt active power filters and SAPFs) are increasingly favoured where harmonic spectra are variable and dynamic, especially in grids with high penetration of power-electronic interfaces (Dehaghani et al., 2026). Recent SAPF implementations and experiments continue to demonstrate substantial harmonic

suppression and power-quality enhancement when suitable reference extraction and current control are applied (Bielecka, 2024; Gaiceanu et al., 2025).

Notwithstanding their effectiveness, SAPFs are constrained by converter rating and cost, switching/conduction losses, sensitivity to controller tuning, and practical limits in dynamic compensation under rapidly varying conditions—limitations that motivate research into stronger adaptive control and parameter-tuning frameworks (Bielecka, 2024; Duc et al., 2023). Recent studies show that optimization-assisted and intelligent/adaptive controllers can improve SAPF regulation of the dc-link and reference tracking while maintaining harmonic compliance during nonlinear load variations (Jai & Ouassaid, 2024; Srivastava & Saravanan, 2024).

In this work, a fuzzy gain–enhanced shunt active power filter was developed and evaluated for a medium-voltage (33 kV) distribution-feeder case study in Nigeria (Afaha-Ube substation to Manta 1 feeder), where the uncompensated operating condition exhibits distortion above typical planning targets used for PCC waveform quality. By adaptively boosting the effective filter control gain through fuzzy inference, the approach targeted improved tracking and harmonic cancellation under operating variability, aligning the compensated feeder performance with harmonic-control expectations consistent with IEEE Std 519-2022 planning and assessment practice (IEEE, 2022).

II. RESEARCH METHODOLOGY

2.1 Case study and simulation environment

The case study is a 33 kV medium-voltage feeder linking the Afaha-Ube substation (Bus 1) to the Manta 1 feeder in Abak (Bus 2), with a line length of 32 km and per-phase lumped series parameters $R = 2.1772 \Omega$ and $X = 0.9173 \Omega$, as further depicted in Table 1.

Table 1: Transmission line data

Parameters	values
Line distance (km)	32
Voltage (pu)	1
Resistance (ohms)	2.1772
Reactance (ohms)	0.9173
Impedance (ohms)	1.3231

A time-domain model was built in MATLAB/Simulink (R2024b) for waveform-level harmonic assessment and filter evaluation. For each phase, the feeder was represented as a series impedance

$$Z_\ell = R_\ell + jX_\ell \quad (1)$$

so that (neglecting shunt capacitance for a short MV feeder) the bus relation is

$$V_2(t) = V_1(t) - Z_\ell I_\ell(t) \quad (2)$$

where I_ℓ is the line current (equal to the source current at Bus 1 in the two-bus structure). For harmonic studies, the impedance is frequency-dependent; a common approximation for predominantly inductive reactance is

$$Z_\ell(h) \approx R_\ell + j h X_\ell \quad (3)$$

where $h = 1, 2, \dots, H$, which captures the fact that inductive reactance scales with harmonic order.

2.2 Harmonic modelling and power-quality indices

Nonlinear loads were modelled as drawing non-sinusoidal currents, decomposed via Fourier series:

$$i_L(t) = I_1 \sin(\omega t + \phi_1) + \sum_{h=2}^H I_h \sin(h\omega t + \phi_h) \quad (4)$$

The SAPF objective is to cancel the harmonic component, as expressed in (5).

$$i_h(t) = \sum_{h=2}^H I_h \sin(h\omega t + \phi_h) \Rightarrow i_L(t) = i_1(t) + i_h(t) \quad (5)$$

Performance was quantified using individual harmonic distortion (per order) and total harmonic distortion for both current and voltage, consistent with the thesis metrics set. The commonly used definitions are highlighted in (6) to (9):

$$\text{IHD}_h(\%) = \frac{I_h}{I_1} \times 100 \quad (6)$$

$$\text{VHD}_h(\%) = \frac{V_h}{V_1} \times 100 \quad (7)$$

$$\text{THD}_I(\%) = \frac{\sqrt{\sum_{h=2}^H I_h^2}}{I_1} \times 100 \quad (8)$$

$$\text{THD}_V(\%) = \frac{\sqrt{\sum_{h=2}^H V_h^2}}{V_1} \times 100 \quad (9)$$

Harmonic acceptability was interpreted at the PCC in line with IEEE Std 519-2022, which establishes steady-state voltage/current distortion goals at the PCC for systems with linear and nonlinear loads (IEEE, 2022). The paper also adopted a practical operational benchmark of $\text{THD} < 5\%$ for “stable” signals during mitigation studies.

2.3 Shunt active power filter (SAPF): plant model and control structure

A shunt active power filter injects a compensating current at the PCC such that the source current becomes close to sinusoidal, as expressed in (10):

$$i_s(t) = i_L(t) - i_f(t) \approx i_1(t) \quad (10)$$

hence the ideal compensating reference is

$$i_f^*(t) = i_L(t) - i_s^*(t) \approx i_h(t) \quad (11)$$

That is, the filter current is equal in magnitude and opposite in phase to the harmonic current component. Power stage dynamics (typical VSI-SAPF): with a coupling inductor L_f and resistance R_f , inverter output voltage v_{inv} , and PCC voltage v_{pcc} ,

$$L_f \frac{di_f}{dt} = v_{inv} - v_{pcc} - R_f i_f \quad (12)$$

The dc-link capacitor C_{dc} dynamics can be written as given in (13).

$$C_{dc} \frac{dv_{dc}}{dt} = i_{dc} - i_{loss} \quad (13)$$

and v_{dc} is typically regulated to ensure adequate inverter voltage headroom during compensation (a key practical requirement highlighted in modern SAPF implementations) (Govind et al., 2024).

Reference current extraction (instantaneous power approach): A widely used method is the instantaneous power (p-q, IRP) theory, often implemented in MATLAB/Simulink and experimentally validated in recent SAPF work (Govind et al., 2024; Kumar & Arya, 2024). Using Clarke transformation

$$\begin{bmatrix} x_\alpha \\ x_\beta \end{bmatrix} = \sqrt{\frac{2}{3}} \begin{bmatrix} 1 & -\frac{1}{2} & -\frac{1}{2} \\ 0 & \frac{\sqrt{3}}{2} & -\frac{\sqrt{3}}{2} \end{bmatrix} \begin{bmatrix} x_a \\ x_b \\ x_c \end{bmatrix} \quad (14)$$

instantaneous powers are expressed in (15) and (16).

$$p = v_\alpha i_\alpha + v_\beta i_\beta \quad (15)$$

$$q = v_\alpha i_\beta - v_\beta i_\alpha \quad (16)$$

then oscillatory components \tilde{p}, \tilde{q} (via low-pass separation) generate compensating currents as highlighted in (17):

$$\begin{bmatrix} i_{f\alpha}^* \\ i_{f\beta}^* \end{bmatrix} = \frac{1}{v_\alpha^2 + v_\beta^2} \begin{bmatrix} v_\alpha & v_\beta \\ v_\beta & -v_\alpha \end{bmatrix} \begin{bmatrix} \tilde{p} \\ \tilde{q} \end{bmatrix} \quad (17)$$

The reference is mapped back to abc via inverse Clarke transform and tracked by a switching strategy (e.g., hysteresis current control or PWM). Recent real-time SAPF studies often pair IRP/SRF reference extraction with hysteresis/PWM tracking and dc-link regulation to enhance robustness under load variation (Govind et al., 2024; Barik et al., 2025).

2.4 Fuzzy gain-enhancement layer (SAPF + FIS)

To address fixed-gain/bandwidth sensitivity and improve compensation under load variability, the paper coupled the SAPF output signals into a fuzzy inference system (FIS) implemented in MATLAB's fuzzy logic tool. In the adopted configuration, the SAPF produces intermediate signals (I_{APF}, V_{APF}) which are mapped to corrected ("clean") signals (I_C, V_C) through a nonlinear fuzzy mapping, as expressed in (18):

$$\begin{bmatrix} I_C \\ V_C \end{bmatrix} = \mathcal{F} \left(\begin{bmatrix} I_{APF} \\ V_{APF} \end{bmatrix} \right) \quad (18)$$

Membership functions and rules: triangular membership functions were selected, with three linguistic terms per variable (Low/Medium/High) for both inputs and outputs. A standard triangular MF is (19).

$$\mu_\Delta(x; a, b, c) = \begin{cases} 0, & x \leq a \\ \frac{x-a}{b-a}, & a < x \leq b \\ \frac{c-x}{c-b}, & b < x < c \\ 0, & x \geq c \end{cases} \quad (19)$$

The rule base comprises 81 inference rules, explicitly documented as mapping (I_{APF}, V_{APF}) \rightarrow (I_C, V_C). Inference and defuzzification (Mamdani form): for rule k , firing strength can be expressed as (20).

$$\alpha_k = \min \{ \mu_{A_k}(I_{APF}), \mu_{B_k}(V_{APF}) \} \quad (20)$$

The aggregation uses a max operator over rules, and centroid defuzzification yields the crisp output (for each output channel $y \in \{I_C, V_C\}$):

$$y^* = \frac{\int y \mu_{out}(y) dy}{\int \mu_{out}(y) dy} \quad (21)$$

This "intelligent layer" concept aligns with current SAPF research trends, which use adaptive and fuzzy

components to improve dc-link regulation, reference tracking, and harmonic suppression under disturbances (Barik et al., 2025; Gupta et al., 2024).

A convenient way to interpret the fuzzy stage in a gain-boost sense is through an effective scaling factor (with saturation to ensure converter limits):

$$k_g(t) = \text{sat} \left(\frac{I_C(t)}{I_{APF}(t) + \epsilon} \right) \quad (22)$$

$$i_f^*(t) = k_g(t) i_{f,APF}^*(t) \quad (23)$$

where ϵ avoids division by zero, this expresses mathematically how fuzzy "correction" can translate into adaptive amplification of the compensating current command.

2.5 Model of the APF and Configuration of the FLM

The APF employed in this research was a Multiple Feedback Active Power Filter (MFAPF), chosen for its ability to enhance selectivity and provide effective band-pass filtering, both of which were critical for accurately modelling power system networks. The initial step in implementing the MFAPF involved transforming the load current into a three-phase (abc) frame current signal, from which the reference current was derived, as expressed in equation (24).

$$i_{ref} = i_{fundamental\ load} - i_{abc\ load} \quad (24)$$

Equation (24) demonstrates that the APF injects a current signal equal in magnitude but opposite in phase to the harmonic load current, thereby ensuring that the source current remains purely sinusoidal and aligned with the voltage signal. At the Point of Common Coupling (PCC), this compensation maintains voltage quality and stability, effectively minimizing harmonic distortion and preserving the integrity of the power system.

$$V_{APF} = V_{source} - V_{load} \quad (25)$$

The APF-filtered voltage and current signals were used as inputs to the FLM.

The procedure utilized for the configuration of the FLM using MATLAB is shown in the outlined steps as follows:

Step 1: Enter V_{APF} and I_{APF} as input to the FLM.

The V_{APF} and I_{APF} were coded and exported from the MATLAB file to the fuzzy logic tool (FLT) in MATLAB R2024b. The fuzzy-logic environment with input variables is shown in Fig. 1. Where I_C and V_C represent the clean current and voltage signal from the FLM model and I_{APF} , and V_{APF} represents the input current and voltage output from the APF.

Step 2: Select the type and the number of membership functions. The snapshot of the

membership for the current signal input is depicted in Fig. 2.

A triangular membership function was selected for this study, with three membership functions assigned to each input and output variable to ensure

effective representation and accurate fuzzy-logic processing.

Step 3: Generate the inference rules. The snapshot of the inference rules is presented in Fig. 3.

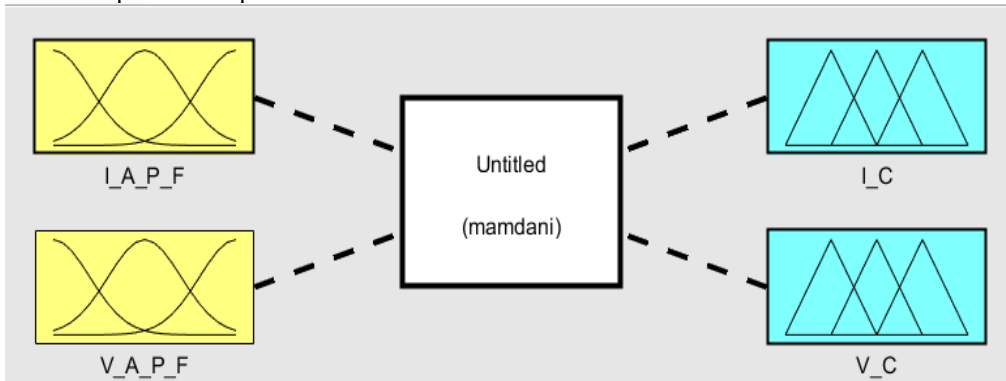


Fig. 1. Image of the FLM environment with input variables

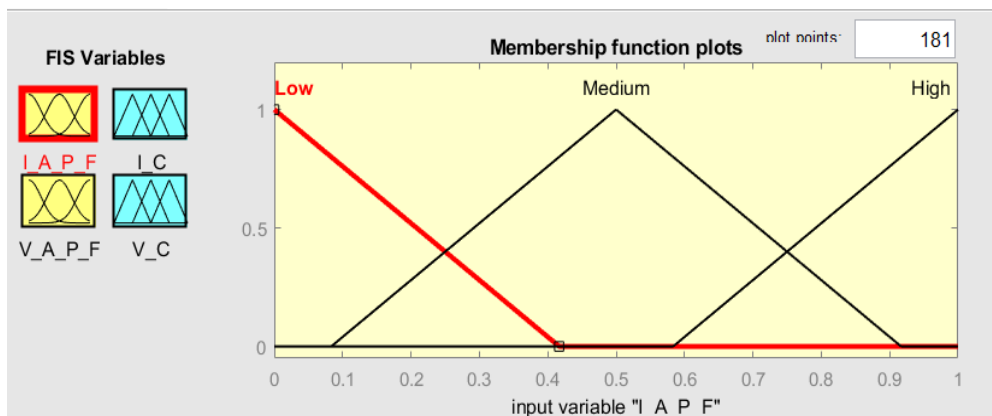


Fig. 2. Image of the membership function for the input current signal

1. If (I_A_P_F is Low) and (V_A_P_F is Low) then (I_C is Low)(V_C is Low) (1)
 2. If (I_A_P_F is Low) and (V_A_P_F is Medium) then (I_C is Low)(V_C is Low) (1)
 3. If (I_A_P_F is Low) and (V_A_P_F is High) then (I_C is Low)(V_C is Low) (1)
 4. If (I_A_P_F is Medium) and (V_A_P_F is Low) then (I_C is Low)(V_C is Low) (1)
 5. If (I_A_P_F is Medium) and (V_A_P_F is Medium) then (I_C is Low)(V_C is Low) (1)
 6. If (I_A_P_F is Medium) and (V_A_P_F is High) then (I_C is Low)(V_C is Low) (1)
 7. If (I_A_P_F is High) and (V_A_P_F is Low) then (I_C is Low)(V_C is Low) (1)
 8. If (I_A_P_F is High) and (V_A_P_F is Medium) then (I_C is Low)(V_C is Low) (1)
 9. If (I_A_P_F is High) and (V_A_P_F is High) then (I_C is Low)(V_C is Low) (1)
 10. If (I_A_P_F is Low) and (V_A_P_F is Low) then (I_C is Medium)(V_C is Low) (1)
 11. If (I_A_P_F is Low) and (V_A_P_F is Medium) then (I_C is Medium)(V_C is Low) (1)

If I_A_P_F is and V_A_P_F is Then I_C is and V_C is

Low Medium High none Low Medium High none Low Medium High none Low Medium High none

not not not not

Fig. 3. Snapshot of the inference rules

The full interpretation of the inference rules in Fig. 3. A total of 81 inference rules were generated, showing the relationship between the input and output variables. The output variable was the least distorted current and voltage signal of the power system network. By direct interpretation, the first row of Fig. 3 implies ‘If I_{APF} is Low and V_{APF} is Low, then I_C will be low, and V_C will be Low.’ For the second row, ‘If I_{APF} is Medium and V_{APF} is Low, then I_C will be low, and V_C will be Low’ and so on. Hence, the current and voltage signals from the APF were sent to the FLM for further harmonic distortion mitigation. The distortion was measured using total harmonic distortion to determine its level.

2.6 Simulation cases and evaluation protocol

Three operating cases were simulated on the same feeder model to enable controlled comparison: (i) uncompensated baseline, (ii) feeder with standalone SAPF, and (iii) feeder with SAPF + fuzzy enhancement. Harmonic spectra (via IHD) and THD were evaluated at both buses (Bus 1 and Bus 2).

III. RESULTS AND DISCUSSION

3.1 Baseline harmonic profile (uncompensated feeder)

Under nonlinear loading and without mitigation, the simulated waveforms at both buses exhibit pronounced distortion with dominant low-order harmonics. The harmonic-order assessment shows that the 7th harmonic dominates phases A and B, while phase C shows strong 3rd-harmonic content, consistent with typical residential/commercial nonlinear load signatures and harmonic propagation along MV feeders. Fig. 4 shows a visibly distorted current waveform at Bus 1, confirming that

harmonic-producing loads inject non-sinusoidal current into the network.

From the harmonics of the current signal monitored for bus 1, it is observed that phases A and C have harmonics up to the 7th order, while phase C has 3rd-order distortion harmonics.

Fig. 5 presents the voltage waveform distortion at Bus 1 under nonlinear loading conditions and without any harmonic mitigation device. While Fig. 4 established that current harmonics are injected into the system, Fig. 5 demonstrates the direct consequence of those harmonic currents on the voltage profile.

For the voltage harmonics distortion signal in Fig. 5, it is observed that phase A has 5th-order harmonics, phase C has 4th-order harmonics, and phase B has 2nd-order harmonics.

Fig 6 and Fig. 7 extend the “without filter” assessment downstream to Bus 2 (Abak feeder) and are important because they show how harmonic effects propagate along the 32 km 33 kV line from Bus 1 to Bus 2. The figures confirm that harmonic distortion is not localized; rather, it travels through the network and appears at the receiving-end bus as both current and voltage harmonics (due to network impedance). From the current signal of bus 2 shown in Fig. 6, it is seen that during the monitoring phase, A and C exhibited 7th-order harmonics, and B exhibited 5th-order harmonics. Also, from Fig. 7, it is seen that during the monitoring phase, A and C had 5th-order harmonics, while B had 4th-order harmonics. The power system monitoring of the 33kV system, illustrated in Fig. 4-7, showed that the rate of distortion with the filter and fuzzy-logic boost was high due to disturbances in the area. Hence, a means of harmonic distortion reduction is necessary; otherwise, the fault may cascade.

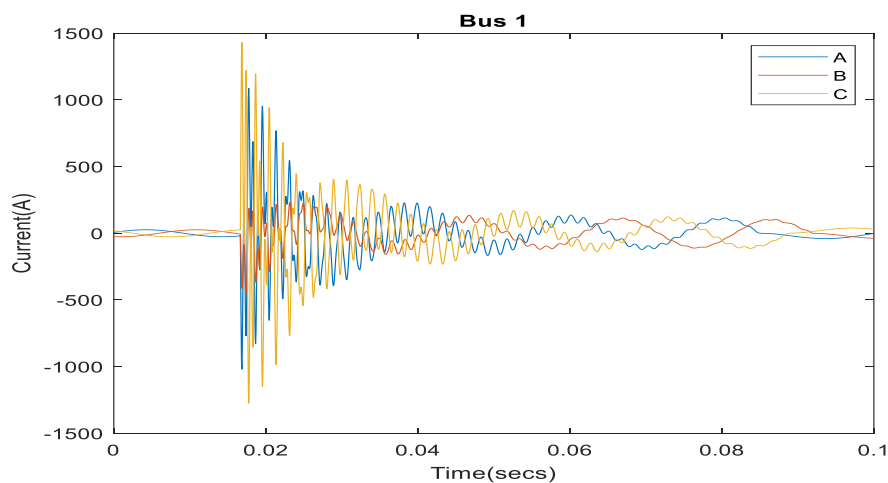


Fig. 4. Harmonic distortion order of the transmission line using current signal for bus 1

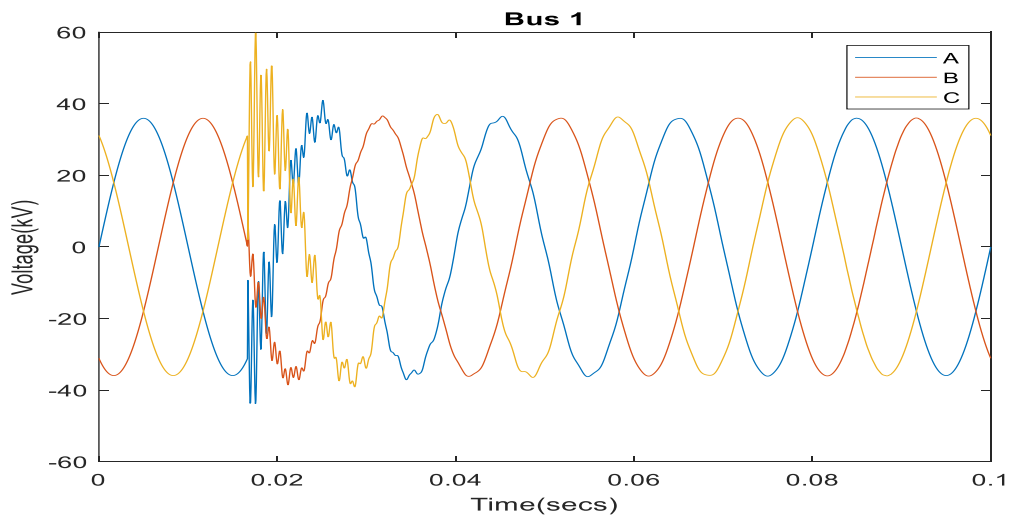


Fig.5. Harmonic distortion order of the transmission line using voltage signal for bus 1

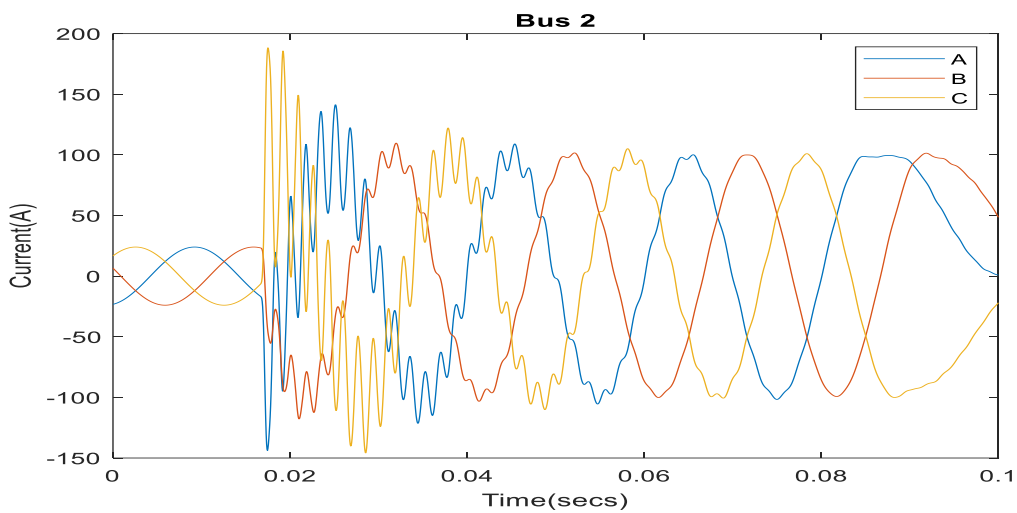


Fig. 6. Harmonic distortion order of the transmission line using current signal for bus 2

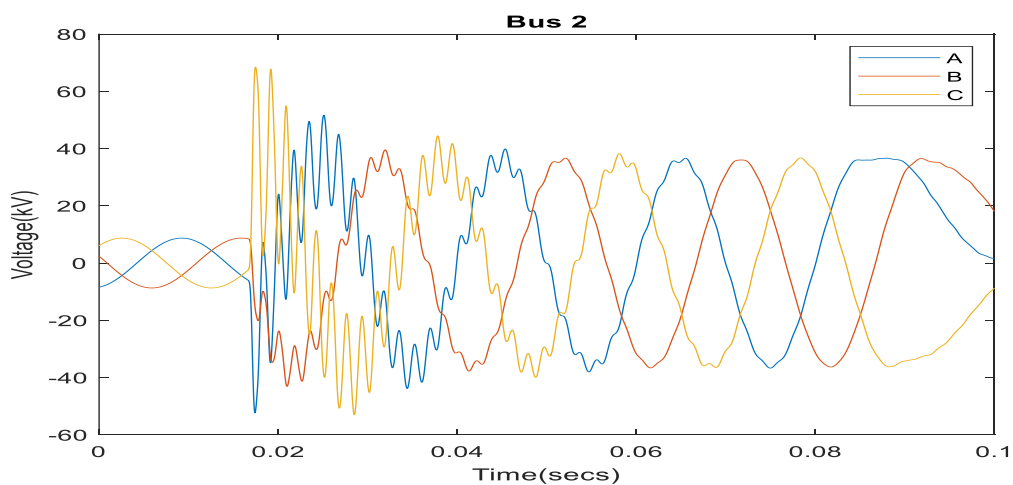


Fig. 7. Harmonic distortion order of the transmission line using voltage signal for bus 2

Quantitatively, Table 1 reports the baseline THD levels: Bus 1: THD_I = 12.31%, THD_V = 9.41% and Bus 2: THD_I = 12.87%, THD_V = 8.99%. These voltage-distortion levels exceed the IEEE Std 519-2022 planning limit commonly applied at the PCC for 1 kV < V ≤ 69 kV (individual harmonic 3%, voltage THD 5%).

Fig. 8 (a) provides quantitative confirmation of the waveform distortions already evidenced qualitatively in Fig. 4 to Fig. 7. In other words, while the earlier plots showed how the current waveform was distorted, Fig. 8 quantifies the severity of the distortion using THD.

Fig 8 (b) complements Fig 8 (a) by shifting from current distortion to voltage distortion, thereby completing the power-quality picture of the system under the unmitigated (no filter) condition. Specifically, the figure summarises the THD of the bus voltages under the nonlinear loading condition with no compensating device installed.

3.2 Standalone shunt active power filter (SAPF) performance

With the SAPF applied at the PCC, the distortion drops below the frequently used operational benchmark of THD < 5% used in the study as the “stable” threshold for acceptable waveform quality. Specifically, Bus 1 improves to THD_I = 4.19%, THD_V = 3.65% while Bus 2 improves to THD_I = 4.23%, THD_V = 3.01%.

To express mitigation strength beyond raw THD, we defined a THD-reduction efficiency as in (25).

$$\eta(\%) = \frac{\text{THD}_0 - \text{THD}_c}{\text{THD}_0} \times 100 \quad (25)$$

and a distortion improvement factor, as expressed in (26).

$$\gamma = \frac{\text{THD}_0}{\text{THD}_c} \quad (26)$$

where THD₀ is the uncompensated THD and THD_c is the compensated THD. Using the reported values, the SAPF achieves $\eta \approx 66\%$ reduction for current THD at both buses (and $\eta \approx 61\%–67\%$ reduction for voltage THD), corresponding to $\gamma \approx 2.6–3.0 \times$ improvement in THD magnitude.

These outcomes align with recent SAPF literature, which shows that properly regulated DC-link/current control yields substantial THD suppression under nonlinear loading (Govind et al., 2024; Gaiceanu et al., 2025).

With the introduction of the Active Power Filter (APF), Figs. 9-12 represent the first stage of harmonic mitigation. These figures collectively show the waveform-restoration effect of the APF alone, without fuzzy-logic enhancement.

The impact of the implementation of the active filter on the transmission system for current signal at bus 1 is presented in Fig. 9. It is observed that the introduction of the filter improved the harmonics of the system and created a near sinusoidal wave, which lowered the harmonic distortion in the bus. Similarly, the introduction of the filter improved the system’s harmonics and produced a near-sinusoidal wave, thereby reducing the voltage harmonic distortion in the bus.

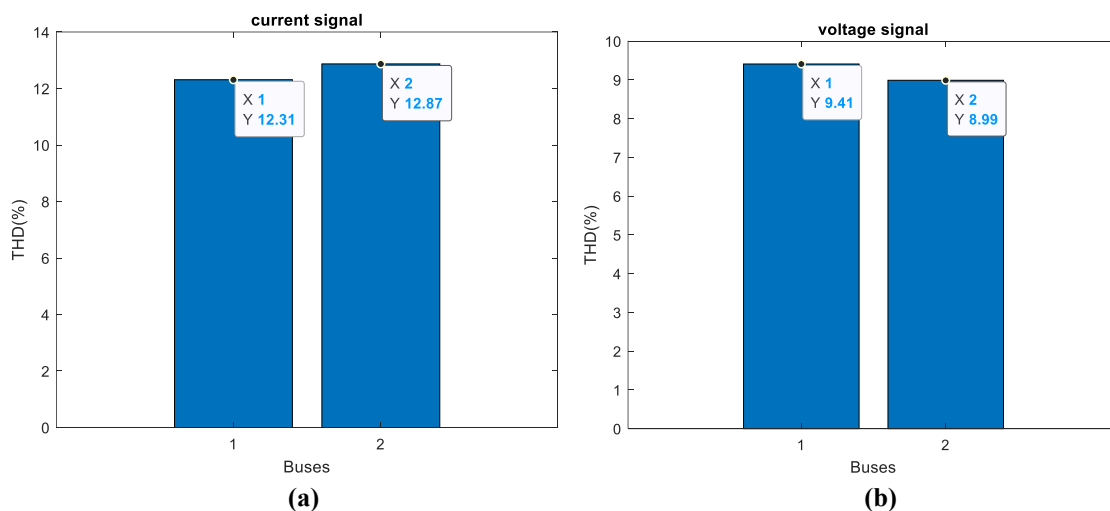


Fig.8. THD of the signal without filter (a) current (b) voltage

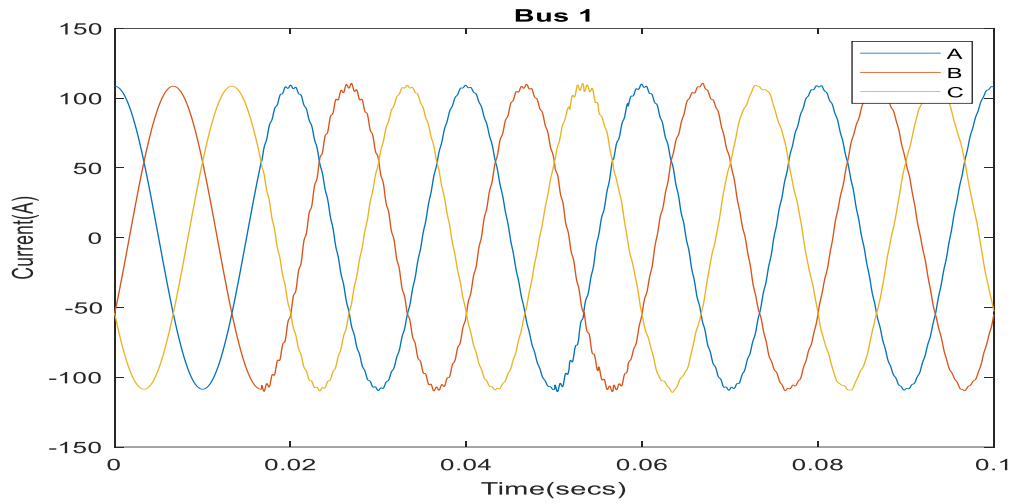


Fig.9. Current signal harmonics of the system with active filter for bus 1

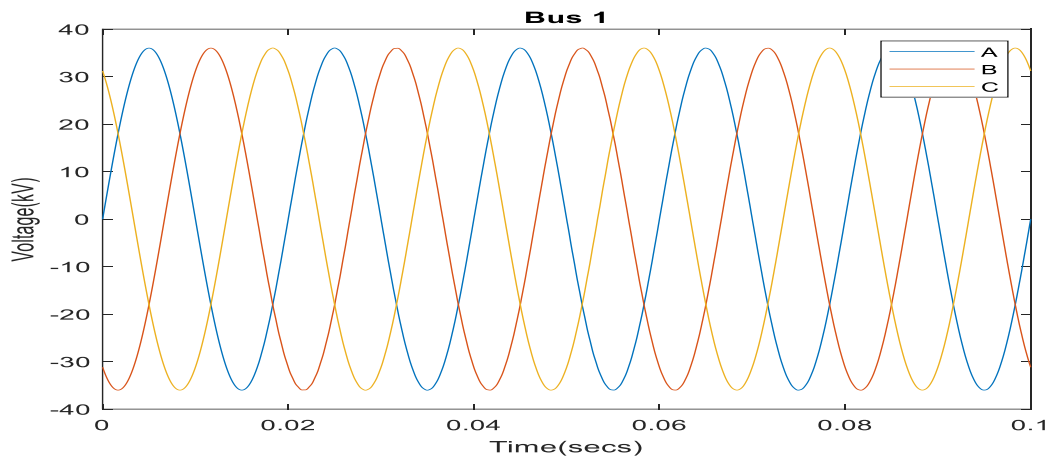


Fig.10. Voltage signal harmonics of the system with active filter for bus 1

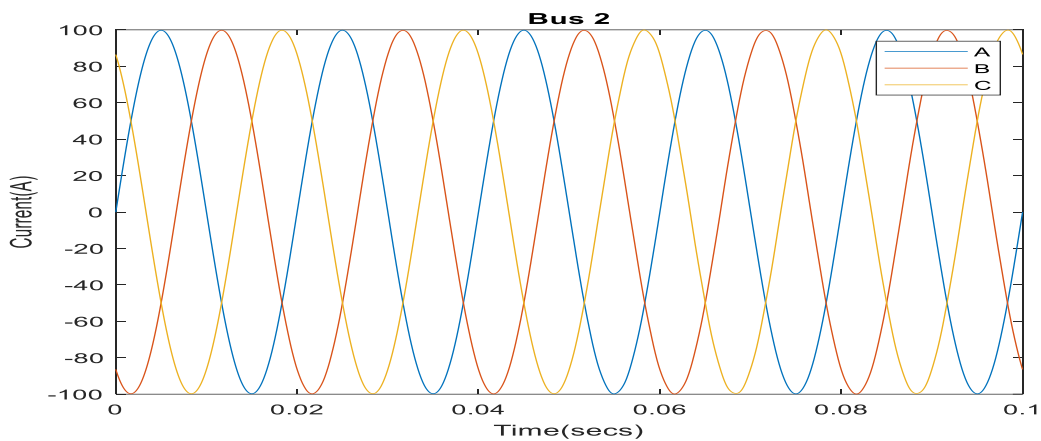


Fig. 11. Current signal harmonics of the system with active filter for bus 2

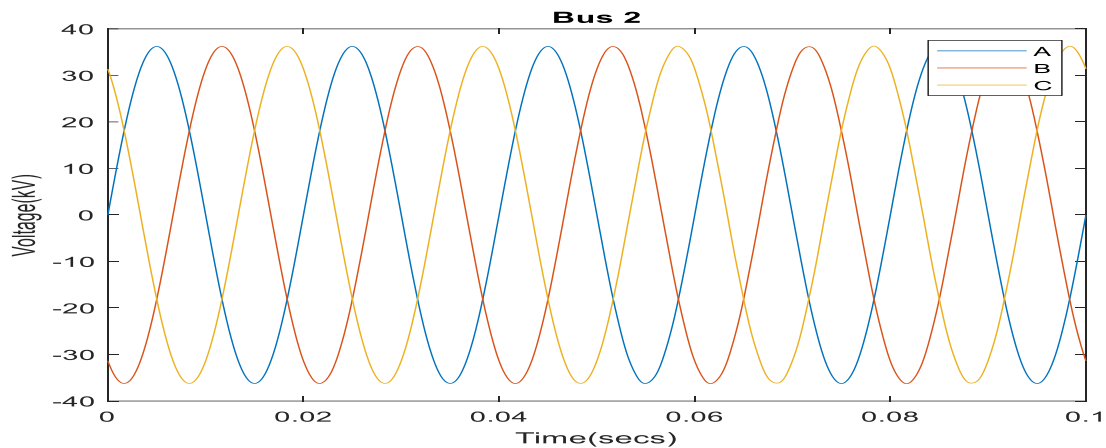


Fig.12. Voltage signal harmonics of the system with active filter for bus 2

The THD of the current signal for the buses with the filter is presented in Fig. 13 (a). From Fig. 13 (a), it is observed that the introduction of the active filter reduced the harmonic distortion of the current signal of the buses to the THD values of 4.19% and 4.23% which are below the threshold of the THD (5%) required for a smooth operation of the power system network.

The THD of the voltage signal for the buses with the filter was shown in Fig. 13 (b). From Fig. 13 (b), it is seen that the introduction of the active filter reduced the harmonic distortion of the voltage signal of the buses to the THD values of 3.65% and 3.01% which are below the threshold of the THD required for a smooth operation of the power system network.

3.3 Fuzzy gain-enhanced SAPF (SAPF-FLC) performance

Figs 14–17 show harmonic response with APF with Fuzzy Logic Controller (hybrid system). These figures show the performance of the hybrid compensation system, which enhances the APF using a Fuzzy Logic Controller (FLC). Unlike the previous stage, where the APF alone reduced THD to acceptable levels (~4%), these figures demonstrate the impact of intelligent gain tuning and adaptive control.

From Figures 14-17, the dynamics are quite the same with the harmonics, with THD = 0. However, minor ripples indicate the presence of distortion in the 3rd-order harmonics.

The THD of the current signal harmonics for buses with a hybrid active filter and fuzzy logic model is shown in Fig. 18 (a). The outcome in Fig. 18 (a) shows that integrating the fuzzy logic model as a boost to the active filter reduced the current

harmonic distortion, with THD below 1%. This implies that the utilization of fuzzy logic remains essential in improving the harmonics of the power system network. The THD of the voltage signal harmonics for buses with a hybrid active filter and fuzzy logic model is shown in Fig. 18 (b). The outcome in Fig. 18 (b) shows a reduction of harmonic distortion to less than 2% due to the introduction of the fuzzy logic model as a boost to the active filter.

Adding the fuzzy gain-enhancement layer produces near-ideal distortion levels. From Table 1, the hybrid SAPF-FLC achieves $THD_I = 0.48\%$ and $THD_V = 1.11\%$ on Bus 1, and $THD_I = 0.67\%$ and $THD_V = 0.97\%$ on Bus 2. Compared with the uncompensated case, current distortion is reduced by ~96.1% at Bus 1 and ~94.8% at Bus 2, while voltage distortion drops by ~88–89%, i.e., comfortably within IEEE 519 voltage THD planning levels for the 33 kV class. A compact way to express the fuzzy “boost” effect on the SAPF command is via an effective adaptive gain acting on the compensating current reference:

$$i_f^*(t) = k_g(t) i_{f,SAPF}^*(t) \quad (27)$$

$$k_g(t) = \text{sat} \left(\frac{I_C(t)}{I_{SAPF}(t) + \epsilon} \right) \quad (28)$$

where I_{SAPF} is the SAPF output signal, I_C is the fuzzy-corrected signal, and ϵ avoids singularity. This representation emphasizes that the fuzzy layer behaves as a nonlinear, bounded amplifier that improves tracking under varying harmonic “error conditions,” consistent with modern adaptive SAPF directions (e.g., fuzzy/adaptive frequency controllers or AI-aided controllers).

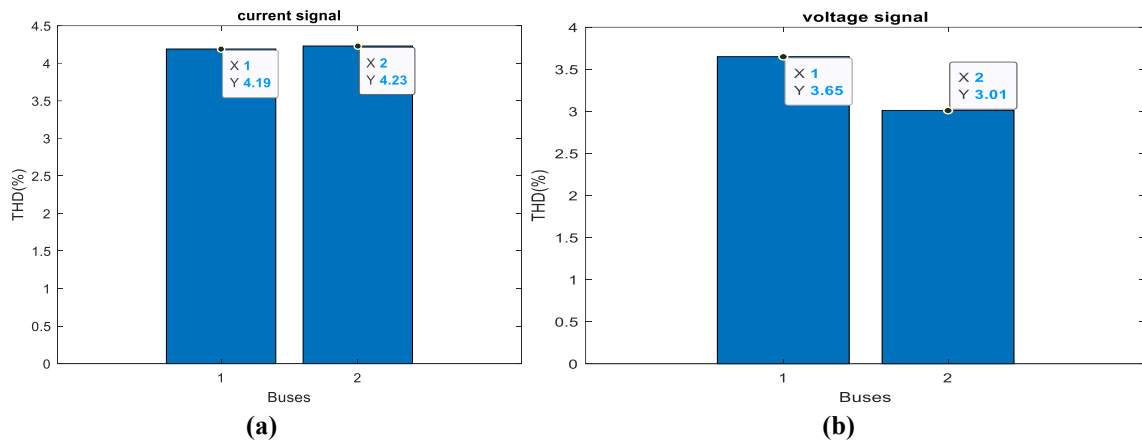


Fig.13. THD of the signal without filter (a) current (b) voltage

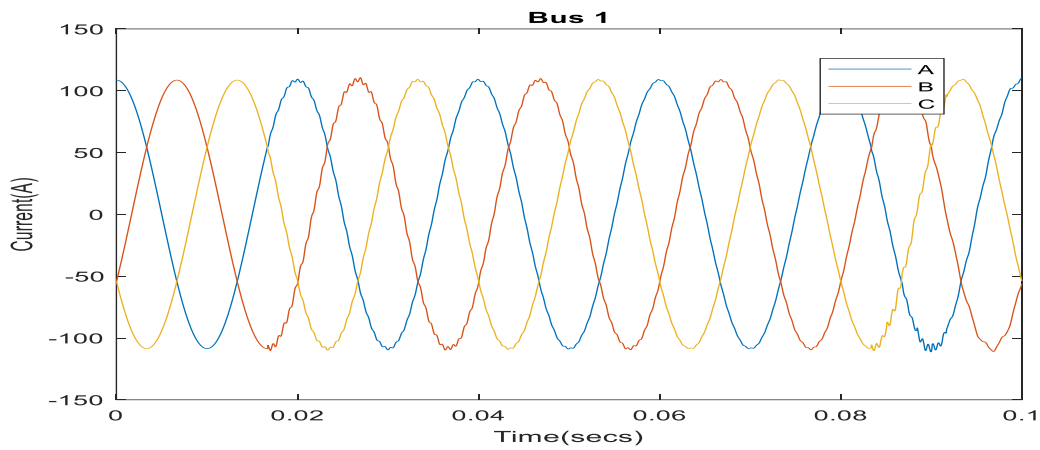


Fig.14. Harmonic distortion of the current signal for bus 1 using active filter and fuzzy logic

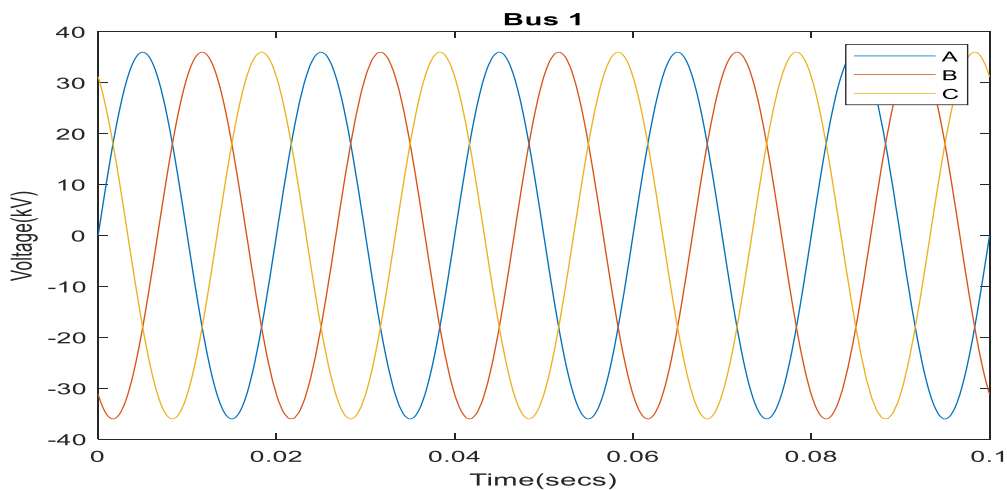


Fig.15. Harmonic distortion of the voltage signal for bus 1 using active filter and fuzzy

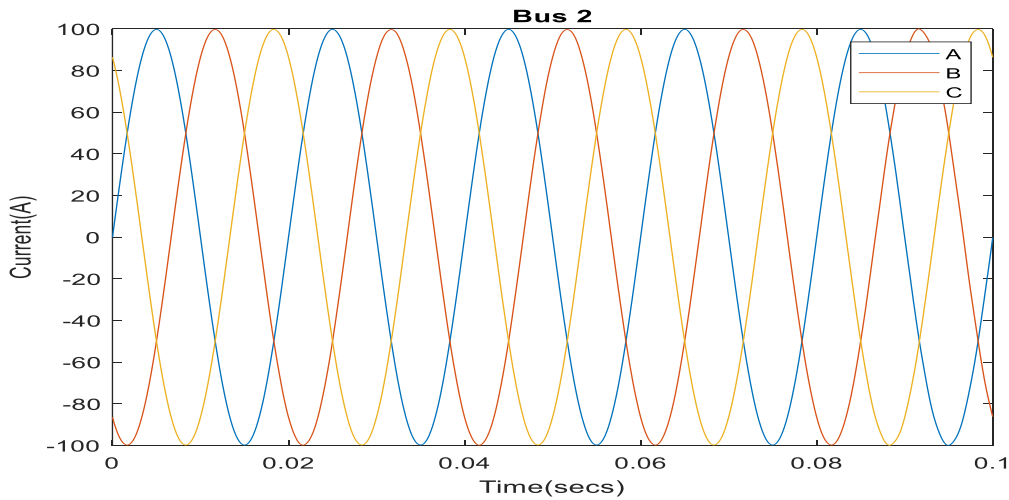


Fig.16. Harmonic distortion of the current signal for bus 2 using active filter and fuzzy logic

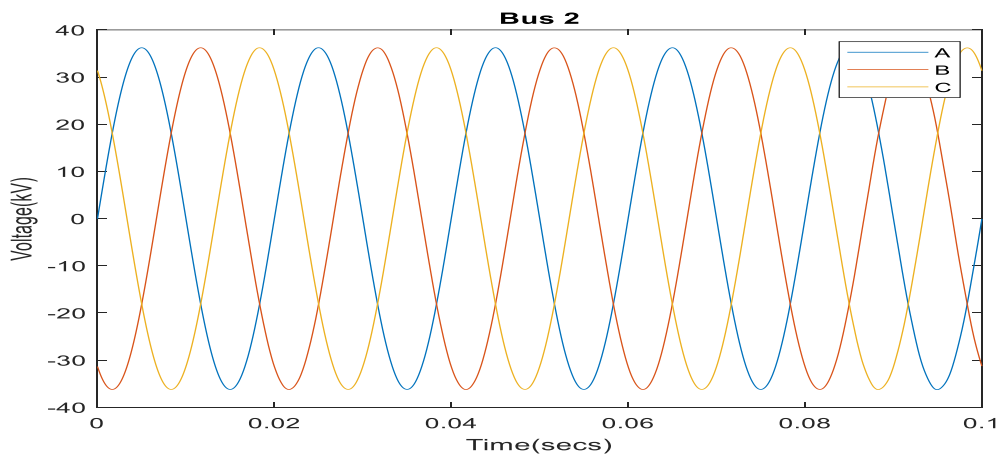


Fig.17. Harmonic distortion of the voltage signal for bus 2 using active filter and fuzzy logic

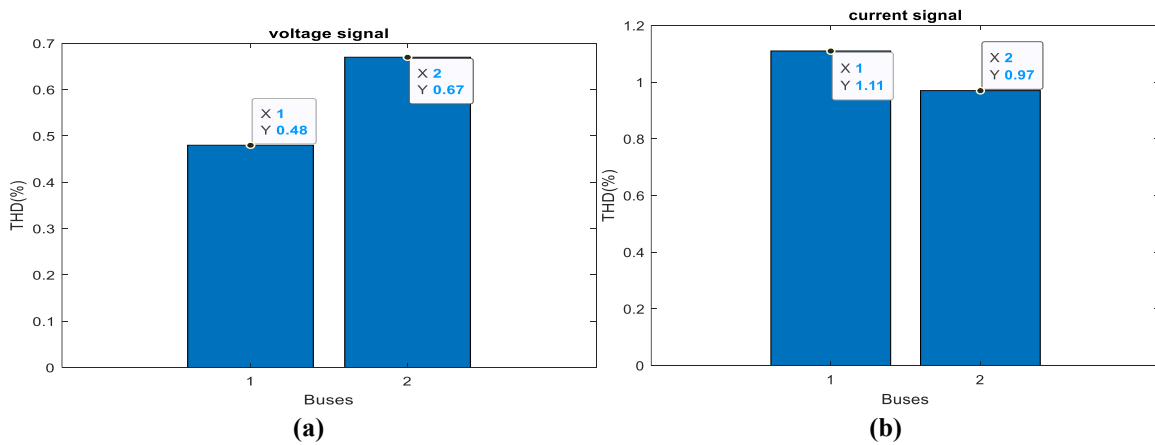


Fig.18. THD of the signal without filter (a) current (b) voltage

3.4 Consolidated THD summary and benchmarking

Table 1 presents the THD results at Bus 1 and Bus 2 under three scenarios (uncompensated, SAPF only, SAPF-FLC).

In comparison with recent studies: (i) experimental/prototype SAPFs often demonstrate THD suppression from ~25–30% down to low single digits depending on controller and operating conditions (Gaiceanu et al., 2025), and (ii) fuzzy-controlled SAPF simulations have reported source-current THD reduced to sub-1% levels (e.g., 0.83%) in nonlinear-load test systems (Cornelius et al., 2024). The present feeder study extends this “sub-1% class” performance to a 33 kV, 32 km MV distribution-feeder case with measurable improvement beyond the standalone SAPF stage.

Limitations and future work. The present validation is simulation-based and employed a reduced feeder representation; future studies should:

- i. Validate on hardware-in-the-loop or field measurements
- ii. Report emission compliance using TDD and short-circuit ratio categories, as emphasized by IEEE 519
- iii. Examine resonance/interharmonics and parameter uncertainty, and
- iv. Benchmark fuzzy gain adaptation against other recent adaptive SAPF control strategies (e.g., frequency-adaptive PIR/PR and data-driven controllers) under identical operating scenarios.

Table 1. THD results at Bus 1 and Bus 2 under three scenarios

Operating condition	Bus 1 THD I (%)	Bus 1 THD V (%)	Bus 2 THD I (%)	Bus 2 THD V (%)
Without filter	12.31	9.41	12.87	8.99
With SAPF	4.19	3.65	4.23	3.01
With SAPF + FLC	0.48	1.11	0.67	0.97

Table 2. Comparative analysis of the proposed study with existing studies

Research paper	Application/system context	Control / key idea	Validation	Reported THD outcome	Key difference vs your proposed work
Ghanayem et al. (2024)	3-phase SAPF under unbalanced grid + nonlinear loads	Frequency-adaptive PIR + voltage-sensorless reference generation; validated on dSPACE	MATLAB/Simulink + real-time dSPACE experiments	Example cases: THD \approx 50.8% \rightarrow 18.4% (rectifier + R load), and 6.16% \rightarrow 3.19% (combined loads)	Strong on frequency variation + sensor reduction; your work targets MV feeder (33 kV, 32 km) case study and achieves sub-1% current THD with a fuzzy gain layer.
Srivastava & Saravanan (2024)	SAPF for EV charging power-quality mitigation	“Optimal design” of SAPF control for dc-link regulation (optimization-based comparison vs other metaheuristics)	MATLAB/Simulink simulation	THD 26.72% \rightarrow 4.33%	Focused on EV charging station and optimization benchmarking; your work demonstrates network-level MV feeder mitigation and pushes THD below 1% using SAPF + fuzzy gain correction.
Fazal et al. (2025)	PV + battery integrated shunt	Energy management	MATLAB simulations +	THD 17.80% \rightarrow	Excellent THD in a converter-

Research paper	Application/system context	Control / key idea	Validation	Reported THD outcome	Key difference vs your proposed work
	active filter (SAF) for grid PQ	(PEMS) with common control strategy, including harmonic mitigation	industrial lab validation	0.68%	integrated SAF architecture; your contribution is fuzzy gain enhancement on a conventional SAPF applied to a 33-kV distribution feeder case study.
Bakria et al. (2025)	SAPF design/control under nominal unbalanced dynamic loads	Golden Jackal Optimizer tunes anti-windup PI + output filter; compares against state-of-the-art	MATLAB/Simulink (as reported in the paper's methods/abstract)	Comparative statement reports THD 0.86% for proposed optimized SAPF vs 3.86% for a GA-optimized PR baseline	Optimization-centric (controller + filter parameter tuning); your approach is rule-based fuzzy gain correction layered on SAPF outputs, validated on MV feeder buses (Bus 1/Bus 2)
Cheepati et al. (2025)	Shunt Active Harmonic Compensator (distribution PQ focus)	New AUV-PQ-SRF reference extraction + OSV-MPC tracking + SMC dc-link regulation	Simulation (IEEE-519-2022 compliant evaluation, per paper)	Paper table reports THD \approx 1.80–1.84% for proposed combined method	Strong on reference extraction + MPC + sliding-mode; your work is comparatively simpler control stack (SAPF + fuzzy gain map) but demonstrates sub-1% current THD on a 33-kV feeder case.
Gaiceanu et al. (2025, Energies 18(23))	Comparative study of direct vs indirect APF control strategies on prototypes	Multiple strategies (PQ, DQ, MAX, LPF, etc.) implemented on FPGA/high-speed platforms	Simulation + experimental test bench + industrial prototypes	Examples reported: THD _i 28.9% → 4.3% (one case) and THD _U 1.1% → 0.3%, THD _I 28.9% → 5.6% (tabulated)	Broad benchmark of control families and hardware realization; your work is a distribution-feeder case study and adds fuzzy gain enhancement to push current THD below 1%.
Gaiceanu et al. (2025, Energies 18(3))	3-phase SAPF prototype using harmonic component separation (LPF)	Harmonic Component Separation + LPF implemented on prototype/test	Numerical + experimental results	THD _I 27.7% → 3.47% (FFT comparison)	Prototype/control-implementation emphasis at low voltage; your work is MV distribution feeder (33 kV) and

Research paper	Application/system context	Control / key idea	Validation	Reported THD outcome	Key difference vs <i>your</i> proposed work
		bench			targets stronger suppression via SAPF + fuzzy gain enhancement (THD _I ≈ 0.48–0.67%).
Current study (this paper)	33 kV Afaha-Ube → Manta 1 feeder (32 km)	SAPF + fuzzy gain enhancement (SAPF-FLC)	MATLAB/Simulink feeder case study	Bus 1: THD _I 12.31% → 0.48%, THD _V 9.41% → 1.11%; Bus 2: THD _I 12.87% → 0.67%, THD _V 8.99% → 0.97%.	Distinctive contributions: MV feeder case context, bus-to-bus reporting (Bus 1/Bus 2), and clear incremental gain from SAPF-only to SAPF-FLC.

IV. CONCLUSION

This paper investigated harmonic distortion mitigation on a real medium-voltage distribution feeder (33 kV Afaha-Ube-Manta 1) by combining a conventional shunt active power filter (SAPF) with a fuzzy gain-enhancement layer. The methodology focused on restoring near-sinusoidal source current at the PCC through compensating current injection, while using fuzzy inference to adaptively strengthen the compensation action under nonlinear load conditions. In the uncompensated case, the feeder exhibited double-digit current THD and elevated voltage THD at both buses (Bus 1: THD_I = 12.31%, THD_V = 9.41%; Bus 2: THD_I = 12.87%, THD_V = 8.99%). Introducing the standalone SAPF reduced distortion to low single-digit levels (Bus 1: 4.19% / 3.65%, Bus 2: 4.23% / 3.01% for current/voltage THD), and the proposed SAPF-fuzzy scheme further improved performance to sub-1% current THD with ~1% voltage THD (Bus 1: 0.48% / 1.11%; Bus 2: 0.67% / 0.97%). For a 33 kV PCC, these voltage-distortion outcomes are consistent with IEEE-based planning expectations commonly interpreted as 5% voltage THD for ≤69 kV systems. The results indicate that the fuzzy gain-enhancement layer provides a meaningful incremental benefit beyond a fixed-parameter SAPF, pushing the compensated feeder from “acceptable” low single-digit THD to “high-quality” near-sinusoidal conditions. This aligns with contemporary SAPF research trends where adaptive/intelligent control layers are used to improve robustness under dynamic nonlinear loading and grid variations. In practice, the proposed architecture provides a deployable pathway for MV distribution utilities seeking improvements in harmonic compliance without relying on narrowband passive tuning.

REFERENCES

- [1]. Bakria, D., Laouid, A., Korich, B., Beladel, A., Teta, A., Mohammedi, R. D., Elsayed, S., Ali, E., Aeggegn, D., & Ghoneim, S. (2025). An optimized shunt active power filter using the golden Jackal optimizer for power quality improvement. *Scientific Reports*, 15, 1–13. <https://doi.org/10.1038/s41598-025-00204-1>
- [2]. Barik, P. K., Shankar, G., Sahoo, P. K., & Samal, S. (2025). *Simulation and real-time implementation of a combined control strategy-based shunt active power filter in microgrid*. *Sustainable Computing: Informatics and Systems*, 46, 101103. <https://doi.org/10.1016/j.suscom.2025.101103>
- [3]. Bielecka, A. (2024). Advanced control algorithm for shunt active power filter: Enhancing power quality in autonomous grids. *Energies*, 17(23), 6186. [doi:10.3390/en17236186](https://doi.org/10.3390/en17236186)
- [4]. Chahine, K. (2024). *Machine learning in active power filters: Advantages, limitations, and future directions*. *AI*, 5(4), 2433–2460. <https://doi.org/10.3390/ai5040119>
- [5]. Cheepati, K., Parimalasundar, E., Suresh, K., Rivera, M., Rao, M., & others. (2025). Design of a novel shunt active harmonic compensator with AUV-PQ-SRF reference current extraction, OSV-MPC and SMC techniques. *Scientific Reports*, 15, Article 28773. <https://doi.org/10.1038/s41598-025-14259-7>
- [6]. Comsys. (2026). Power quality – IEEE 519-2022 (table summary of IEEE 519-2022 voltage distortion limits).
- [7]. Cornelius, A. P., Ved, N. K., & Muhammad, A. I. (2024, August). *Three-phase shunt active power filter based fuzzy logic controller for the reduction of total harmonic distortion (THD)*. African Scholar Publications.
- [8]. Dehaghani, M. N., Korötko, T., & Rosin, A. (2026). Power quality improvement in DG based distribution systems: A review. *Renewable and Sustainable Energy Reviews*, 225, 116184. [doi:10.1016/j.rser.2025.116184](https://doi.org/10.1016/j.rser.2025.116184)
- [9]. Duc, M. L., Hlavaty, L., Bilik, P., & Martinek, R. (2023). Harmonic mitigation using meta-heuristic optimization for shunt adaptive power filters: A review. *Energies*, 16(10), 3998. [doi:10.3390/en16103998](https://doi.org/10.3390/en16103998)
- [10]. Fazal, M., Alali, M., Phulpin, T., Forestier, R., & Goasguen, C. (2025). Implementation of a priority-based energy management scheme with a common control strategy for PV and battery integrated shunt active filters. *Energy Conversion and Management: X*, 26, 100977. <https://doi.org/10.1016/j.ecmx.2025.100977>
- [11]. Gaiceanu, M., Epure, S., Solea, R. C., & Buhosu, R. (2025). Power Quality Improvement with Three-Phase Shunt Active Power Filter Prototype Based on Harmonic Component Separation Method with Low-Pass Filter. *Energies*, 18(3), 556. <https://doi.org/10.3390/en18030556>
- [12]. Gaiceanu, M., Epure, S., Solea, R. C., Buhosu, R., Vlad, C., & Marin, G.-A. (2025). Comparison of Direct and Indirect Control Strategies Applied to Active Power Filter

- Prototypes. *Energies*, 18(23), 6337. <https://doi.org/10.3390/en18236337>
- [13]. Ghanayem, H., Alathamneh, M., Yang, X., Seo, S., & Nelms, R. M. (2024). Enhanced three-phase shunt active power filter utilizing an adaptive frequency proportional-integral-resonant controller and a sensorless voltage method. *Energies*, 18(1), 116. <https://doi.org/10.3390/en18010116>
- [14]. Govind, A., Jayaswal, K., Tayal, V. K., & Kumar, P. (2024). *Simulation and real time implementation of shunt active power filter for power quality enhancement using adaptive neural network topology*. *Electric Power Systems Research*, 228, 110042. <https://doi.org/10.1016/j.epsr.2023.110042>
- [15]. Gupta, U. K., Sethi, D., & Goswami, P. K. (2024). *Adaptive TS-ANFIS neuro-fuzzy controller based single phase shunt active power filter to mitigate sensitive power quality issues in IoT devices*. *e-Prime—Advances in Electrical Engineering, Electronics and Energy*, 8, 100542. <https://doi.org/10.1016/j.prime.2024.100542>
- [16]. Institute of Electrical and Electronics Engineers. (2022). *IEEE Std 519-2022: IEEE standard for harmonic control in electric power systems*. IEEE Standards Association.
- [17]. Jai, A. A., & Ouassaid, M. (2024). Three novel machine learning-based adaptive controllers for a photovoltaic shunt active power filter performance enhancement. *Scientific African*, 24, e02171. [doi:10.1016/j.sciaf.2024.e02171](https://doi.org/10.1016/j.sciaf.2024.e02171)
- [18]. Kumar, S., & Arya, K. (2024). *Implementation of instantaneous p-q theory to improve power quality by shunt active power filter for non-linear loads* (IEEE ICEPES). (Publication summary page).
- [19]. ScienceDirect Topics. (n.d.). Distortion limit—overview (summarizing IEEE 519 voltage distortion limits at ≤ 69 kV).
- [20]. Seddik, M. S., Eteiba, M. B., & Shazly, J. (2024). Evaluating the harmonic effects on the thermal performance of a power transformer. *Energies*, 17(19), 4871. [doi:10.3390/en17194871](https://doi.org/10.3390/en17194871)
- [21]. Srivastava, A., & Saravanan, S. (2024). Harmonic mitigation using optimal active power filter for the improvement of power quality for an electric vehicle charging station. *e-Prime – Advances in Electrical Engineering, Electronics and Energy*, 8, 100527. <https://doi.org/10.1016/j.prime.2024.100527>